JOURNAL OF MATERIALS SCIENCE 39 (2004) 881–888

Advanced symmetrically graded ceramic and ceramic-metal composites

S. PUT, G. ANNÉ, J. VLEUGELS, O. VAN DER BIEST
Department of Metallurgy and Materials Engineering, Katholieke Universiteit Leuven, Kasteelpark Arenberg 44, B-3001 Leuven, Belgium
E-mail: omer.VanderBiest@mtm.kuleuven.ac.be

The potential of electrophoretic deposition as a shaping process of free-standing objects with a gradient in composition is investigated. The capability to produce relatively thick continuously graded ZrO_2-Al_2O_3 and WC-Co-Ti(C,N) discs was explored. After electrophoretic deposition, the dried deposits were cold isostatically pressed and pressureless sintered. In order to create a symmetric gradient profile along the thickness of the plates, a mathematical model for the EPD process was developed in order to predict the composition and slope of the gradient profile in the discs from the starting composition of the suspension, the EPD operating parameters and the powder-specific EPD characteristics. The sintered graded materials have a continuous variation in composition, microstructure and mechanical properties. In the illustrated ZrO_2-Al_2O_3 example, the ZrO_2 content increases from 0 vol% on the outer surface up to 25 vol% in the core. For the WC-Co-Ti(C,N) discs, the Ti(C,N) content decreases from 5 wt% on the outer edge to 0 wt% in the bulk of the material. In both materials, a hard outer rim and a tough core are obtained. Finally, the residual surface stresses of the densified graded ZrO_2-Al_2O_3 discs were investigated.
© *2004 Kluwer Academic Publishers*

1. Introduction

In today's highly demanding technology environment, wear parts and cutting tools are commonly coated in order to increase their performance. The coating thickness is normally between 1–50 μm, depending on the deposition process, which presents limitations in lifetime or property influence of the relatively soft substrate [1]. A major disadvantage of coated materials is the sharp interface between coating and substrate, often causing delamination during operation. Moreover, coated cutting tools are often exposed to severe thermal stresses during operation. These problems inspired the concept of functionally graded materials (FGM), in which the thermal stresses can be reduced and the coating adherence can be improved by providing a gradual transition in microstructure between the two elastically dissimilar materials [2, 3].

Electrophoretic deposition (EPD) is explored in this paper as a potential processing technique for functionally graded ceramic composites and hardmetals with a continuous gradient profile. Electrophoretic deposition consists of two processes, i.e., the movement of charged particles in a suspension in an electric field between two electrodes (electrophoresis) and particle deposition on one of the electrodes or on a membrane (electrocoagulation). Stable well-dispersed particle suspensions are necessary to produce densely packed deposits by EPD [4]. The green density should be as high as possible to provide a high green strength and enhanced densification during sintering. Numerous applications of EPD have already been developed for the fabrication of ceramics [5], including coatings [6–9], laminated materials [10, 11] and functionally graded materials [12–16]. FGM materials can be obtained since the composition of the deposit is determined by the composition of the suspension at the moment of deposition. Thus by changing the composition of the suspension, gradient materials with a continuously changing composition can be obtained [15].

In this work, suitable suspensions are developed to produce homogeneous Al_2O_3, ZrO_2, WC-Co and Ti(C,N) materials by electrophoretic deposition. Subsequently, functionally graded Al_2O_3/ZrO_2 and WC-Co/Ti(C,N) discs with a symmetrical gradient in respectively ZrO_2 and Ti(C,N) content are processed by means of electrophoretic deposition.

2. Experimental procedure

The powders used, are commercially available 3 mol% Y_2O_3 co-precipitated ZrO_2, Al_2O_3, Ti($C_{0.7}$,$N_{0.3}$), WC-5Co, WC-10Co and WC-12Co. More details are given in Table I. Additionally, WC-10Co-5Ti(C,N) and WC-10Co-10Ti(C,N) powders were prepared by mixing WC-10Co powders with Ti($C_{0.7}$,$N_{0.3}$). All WC-Co powders were doped with VC and attrition-milled from an initial WC-Co agglomerate size of about 50 μm down to a particle size of about 1 μm (Table I). Although the Y_2O_3 co-precipitated ZrO_2 powder has

TABLE I Origin and properties of the different powders used for EPD

Powder	Supplier	Grade	d_{50} (μm)	BET (m^2/g)
ZrO_2	Daiichi, Kigenso Kagaku Kogyo, Japan	HSY-3U	0.35	20
Al_2O_3	Baikowski, France	SM8	0.30	10
$Ti(C_{0.7},N_{0.3})$	H.C. Starck, Germany	B	2.08	1–2
WC-5Co	Nanodyne, Umicore, Belgium	Nanocarb	0.94	2.47
WC-10Co	Nanodyne, Umicore, Belgium	Mycrocarb	1.14	2.19
WC-12Co	Nanodyne, Umicore, Belgium	Nanocarb	1.08	3.23

a particle size of 0.35 μm, it has a crystallite size of 30 nm. The as-received powders were ball milled in ethanol on a multidirectional mixer (type Turbula) for 24 h to break the hard agglomerates. Y-TZP milling balls were used for the ZrO_2-Al_2O_3 composites, whereas a WC-Co milling medium was used for the other suspensions. After milling, the ethanol is evaporated by means of a rotating evaporator and the powder is dried at 90°C for 12 h.

Technical grade acetone (Acros, 99.5%) and *n*-butylamine (Acros, 99.5%) were used as suspension media. The suspensions are mixed by a magnetic stirrer for 15 min and subsequently ultrasonicated in an ultrasonic bath (Branson 2510) for 15 min. An in-house developed deposition set-up, schematically shown in Fig. 1a, was used for the EPD experiments. The polytetrafluorethylene (PTFE) deposition cell contains two parallel flat stainless steel electrodes with a surface area of 9 cm^2. The distance between the electrodes is 3.5 cm. Electrophoretic deposition at constant voltage was performed with freshly prepared suspensions, using a F.U.G. (type MCN 1400-50) power supply.

For the production of ceramic-metal WC-Co/Ti(C,N) FGMs, a WC-Co starting suspension containing acetone and 10 vol% *n*-butylamine was pumped in a circulating system through the deposition cell by a peristaltic pump. A second suspension with WC-Co-Ti(C,N) powder was added to the circulating suspension at well defined times and rates by means of another peristaltic pump, allowing to continuously change the Ti(C,N) concentration from 0 up to about 5 to 10 wt%. The addition rate, i.e., the pumping speed of the second suspension to the circulating suspension, determines

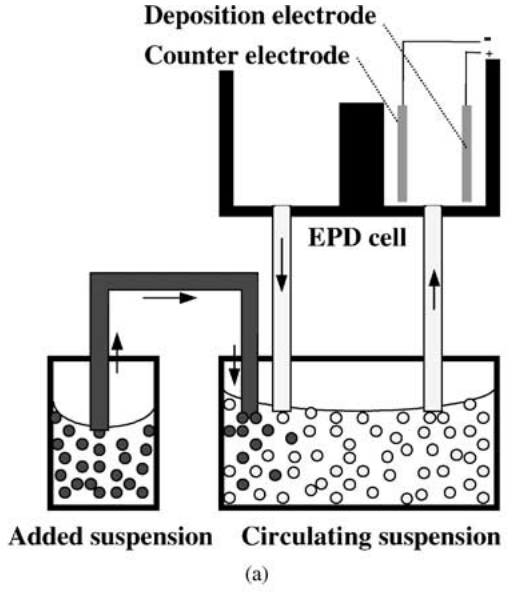

(a)

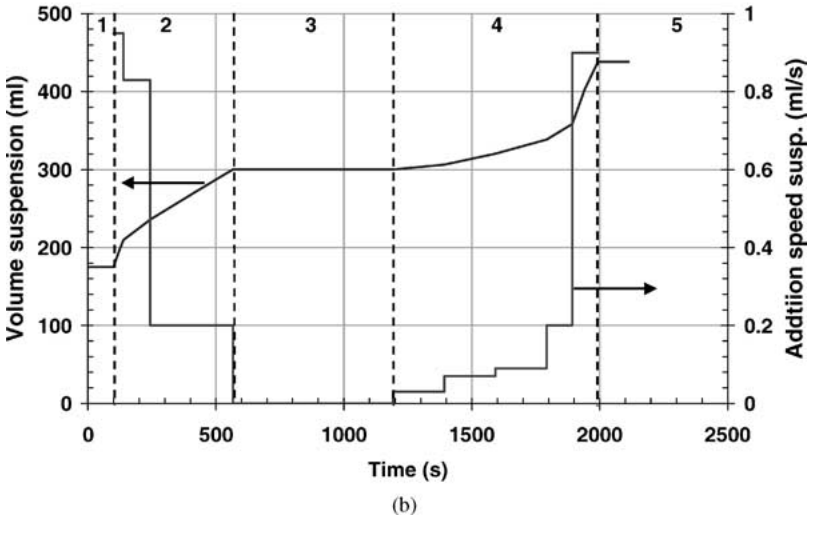

(b)

Figure 1 (a) Schematic view of the EPD set-up for the production of functionally graded materials. (b) Volume and addition rate of the suspensions as a function of time during processing of a double gradient $Al_2O_3/ZrO_2/Al_2O_3$ FGM.

the shape of the Ti(C,N) concentration gradient. In a similar way, Al_2O_3/ZrO_2 FGM plates can be produced by continuously adding a ZrO_2 suspension to a circulating Al_2O_3 suspension. All suspensions were based on acetone with the addition of 10 vol% *n*-butylamine.

In order to produce symmetrically graded FGM plates with a Ti(C,N) rich outer layer and a homogeneous WC-Co core, a WC-Co-Ti(C,N) starting suspension was used to produce the Ti(C,N)-rich outer part. After deposition for a certain time, a second WC-Co suspension was continuously added to the circulating suspension in order to create a decreasing Ti(C,N) content. After addition of the second suspension, EPD is continued until the pre-defined homogeneous core width is reached. Subsequently, a third WC-Co-Ti(C,N) suspension is added, increasing the Ti(C,N) content up to the defined level.

For the deposition of symmetrically graded $Al_2O_3/ZrO_2/Al_2O_3$ discs, a 175 ml starting suspension I, containing 70 g/l Al_2O_3, was pumped through the deposition cell by peristaltic pump 1 at a rate of 2.5 ml/s (see Fig. 1a). After 100 s of deposition, 125 ml of suspension II with 135 g/l of an Al_2O_3/ZrO_2 (70 vol% Al_2O_3) mixture was added to the circulating suspension by pump 2. After 7 min, the addition of suspension II was completed. During the subsequent step, the suspension is circulated and EPD is continued for 630 s without any further additions. Afterwards, 140 ml of suspension III with 150 g/l Al_2O_3 was added at a constant speed for 800 s. In the last step, the remaining suspension was circulated for 120 s. During all the described steps, EPD is continued in the deposition cell. The addition speed of suspension II and III by pump 2 was varied in such a way that a convex concentration profile was obtained in both gradients. The addition speed of the suspensions as well as the volume of suspensions as a function of time are illustrated in Fig. 1b.

The dried green discs were Cold Isostatically Pressed (CIPed) at 300 MPa for 3 min and pressureless sintered. The WC-Co/Ti(C,N) discs were sintered in vacuum for 1 h at 1450°C, whereas the Al_2O_3/ZrO_2 composites were densified in air at 1480°C for 2 h. Microstructural investigation of polished cross-sectioned samples was performed by means of scanning electron microscopy (SEM, XL30-FEG, FEI, Eindhoven, The Netherlands). Quantitative electron probe microanalyses (EPMA, Superprobe 733, Jeol, Tokyo, Japan) were performed with an energy dispersive system (EDS, Tracor Northorn, USA) using reference samples. X-ray diffraction analysis (XRD, 3003-TT, Seifert, Ahrensburg, Germany) of the sintered Al_2O_3/ZrO_2 FGM discs was done using Cu K_α radiation (40 kV, 30 mA) in order to determine the residual stresses in the surface layer of the graded discs. The density of the specimens was measured in ethanol according to the Archimedes method. The Vickers hardness $HV_{0.5}$ and HV_{10} were measured with an indentation load of 0.5 or 10 kg (model 3202, Zwick, Ulm, Germany). The indentation fracture toughness was calculated from the radial cracks originating from the corners of HV_{10} indentations [17].

3. Results and discussion

3.1. Electrophoretic deposition of homogeneous ceramic and metal-ceramic discs

For successful EPD of composite and FGM systems, one needs a stable suspension from which both powders can be deposited on the same electrode with a sufficiently high deposition rate, suitable for making thick deposits. Additional requirements are an adequate smoothness of the deposit surfaces and a high green density. Moreover, the particle size of the powders is important for EPD and has to be kept below 10 μm to avoid sedimentation during deposition. Therefore, all WC-Co powders were attritor milled to a final particle size of about 1 μm.

Important powder properties are the point of zero charge (pzc) and the natural pH of the powders in suspension. The pzc is defined as the pH of the suspension where the powder carries no net charge and can be determined by a potentiometric titration [15]. The natural pH is defined as the pH to which the suspension equilibrates when powder is suspended in demineralised water at a given powder concentration, defined here as 100 g/l. The natural pH can vary due to the presence of impurities that can strongly influence the surface groups on the powder. The powder is negatively charged in demineralised water when the natural pH > pzc and positively charged when pzc > natural pH [15]. Fig. 2 shows the pzc versus natural pH for the powders used. It is shown that the pzc of the Ti(C,N) and ZrO_2 powders is slightly acid, whereas the pzc of Al_2O_3, WC-Co and WC-Co-Ti(C,N) are slightly basic. For all powders, the natural pH does not deviate strongly from the pzc, indicating a limited amount of impurities in the powders, which will not significantly influence the charging behaviour of the powders in the solvents.

Since Y_2O_3 and cobalt dissolve when the acidity of the suspension is too high, alkaline suspensions are preferred for the electrophoretic deposition experiments. Moreover, due to the hydrolysis of water and the concomitant formation of gas bubbles at the stainless steel electrodes at voltages above about 3 V, organic solvent based suspensions are often used for EPD experiments at higher voltages.

Different electrophoretic deposition experiments revealed successful deposition of the powders from

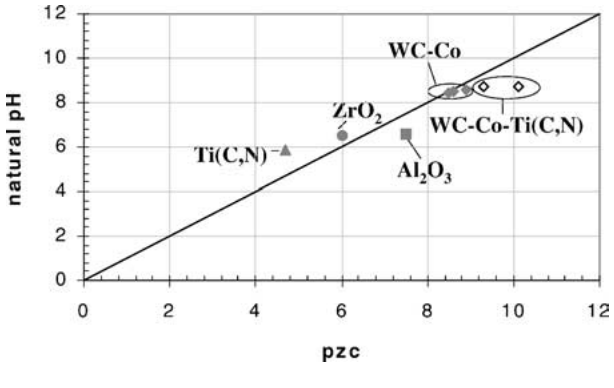

Figure 2 Charging map of the ZrO_2, Al_2O_3, Ti(C,N), WC-Co and WC-Co-Ti(C,N) powders.

TABLE II Electrophoretic mobility and effective particle charge of different powders in an acetone/10 vol% *n*-butylamine suspension

	Electrophoretic mobility[a] (10^{-9} m^2/V·s)	Effective particle charge (mC/g)
Al_2O_3	−15.2	53
ZrO_2	−14.3	40
WC-5Co	−12.7	90
WC-10Co	−12.5	95
WC-12Co	−13.9	85
WC-Co-5Ti(C,N)	−14.9	110
WC-Co-10Ti(C,N)	−14.9	160

[a]Measured after 5 min EPD in a suspension containing 20 g powder.

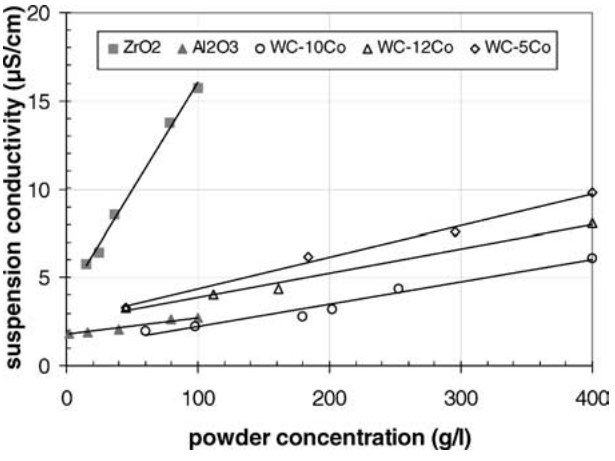

Figure 3 Suspension conductivity S_{sus} as a function of powder in an acetone-based suspension.

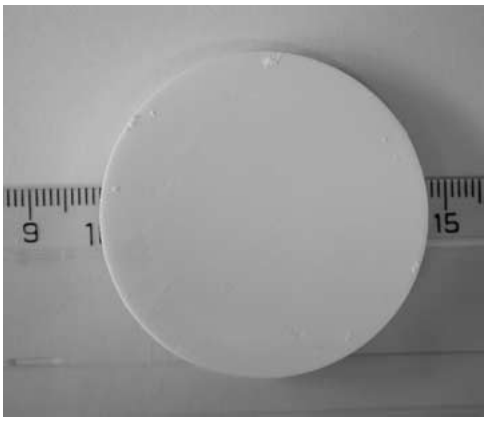

Figure 4 Sintered FGM disc with a sintered thickness of 5 mm and a diameter >30 mm.

acetone with 10 vol% *n*-butylamine, whereas no deposition was observed for the WC-Co powders from ethanol suspensions with acetic acid additions. Investigation of homogeneous powder suspensions was performed in order to determine the electrophoretic mobility of the different powders from the deposition yield, derived from Hamaker's equation [18], assuming a constant electric field:

$$\mu = -\frac{Hd}{tVA}\ln\left(\frac{M-Y}{M}\right) \quad (1)$$

with H, the volume of suspension (m^3), d, the distance between the electrodes (m), t, the deposition time (s), V, the applied voltage (V), A, the surface area of the electrode (m^2), M, the initial powder mass in suspension (g) and Y, the yield of deposition (g). Table II summarises the electrophoretic mobility for the different powders in an acetone-based suspension. The WC-Co-Ti(C,N) powders have a slightly higher mobility than the other WC-Co powders. For the ZrO_2-Al_2O_3 system, Al_2O_3 deposits faster than ZrO_2.

In order to control the EPD behaviour of FGM materials, three important parameters need to be determined on homogeneous powder suspensions. These powder-specific parameters are: (i) the effective charge of the powder in suspension, Q, (ii) the electrophoretic mobility, μ, and (iii) the specific conductivity of the suspension as a function of time or powder concentration, S_{sus}, during the experiment. These parameters can be determined from EPD experiments with homogeneous powder suspensions. The experimentally determined values of the mobility μ and the powder charge Q for the different powders in suspension are given in Table II. Fig. 3 shows the linear decrease of the suspension conductivity as a function of decreasing powder concentration for different powders in an acetone/*n*-butylamine suspension during EPD at different times. Each experiment was repeated 3 times. The powder charge and solvent conductivity, as calculated from the slope and intercept of Fig. 3, are incorporated in the EPD model to predict the gradient profile of FGMs. More details on the model are reported elsewhere [19]. Table II clearly shows that the ZrO_2 powder has a lower powder charge and electrophoretic mobility compared to the Al_2O_3 powder.

The green EPD deposits were removed from the electrode, dried for 1 day in a controlled atmosphere, CIPed and sintered in a controlled atmosphere. The green density of the EPD plates was 40 ± 2% of the theoretical value for the WC-Co and WC-Co-Ti(C,N) discs, whereas the CIPed plates revealed a density of 55%. The Al_2O_3 plates revealed green densities of 55% whereas the ZrO_2 plates showed a relatively low density of 30%. The lower green density value of ZrO_2 could be explained by the lower powder charge Q, indicating that ZrO_2 is less stable in suspension compared to Al_2O_3 (Table II). As a result, the ZrO_2 powder will easier agglomerate and thus form a deposit with a lower green density. After sintering, fully dense plates with a sintered diameter >30 mm and a thickness of 5 mm could be obtained (Fig. 4).

3.2. Electrophoretic deposition of WC-Co/WC-Co-Ti(C,N) FGMs

Based on Hamaker's equation, which states that the amount of powder, Y, brought to the electrode during time t, depends on the electrophoretic mobility, μ, of the powder in suspension, the electrical field strength, E, between the electrodes, the solids loading C of the powder in suspension and the surface area, A, of the electrode, a mathematical model was developed to predict the slope, width and composition of the gradient profile in plate-shaped FGMs from the EPD parameters and

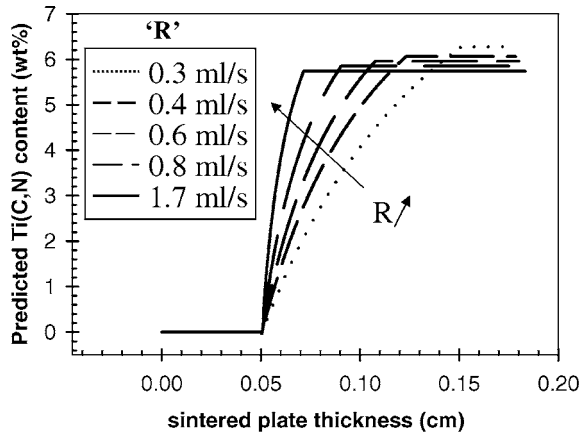

(a)

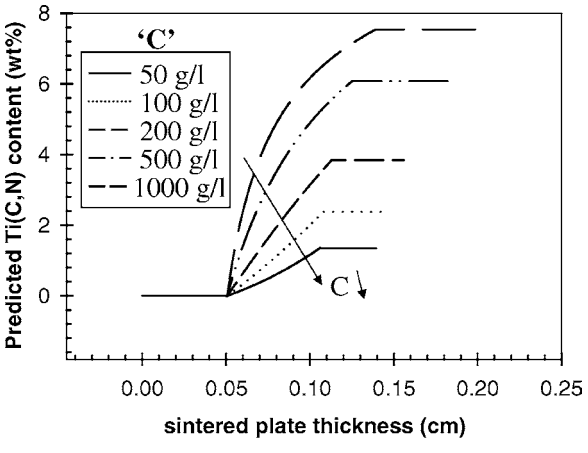

(b)

Figure 5 Influence of the addition rate, R, (a) and powder load (b) of a WC-Co-10Ti(C,N) suspension on the predicted concentration profile when added to a circulating WC-10Co suspension.

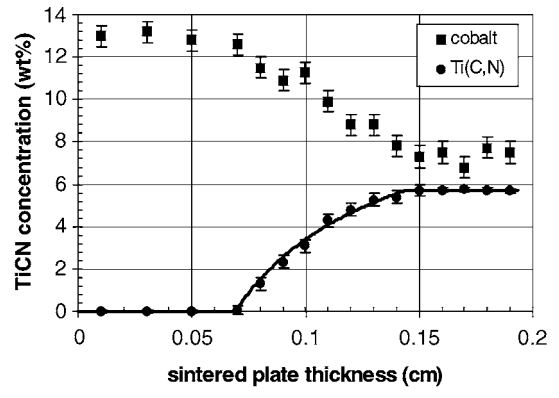

(a)

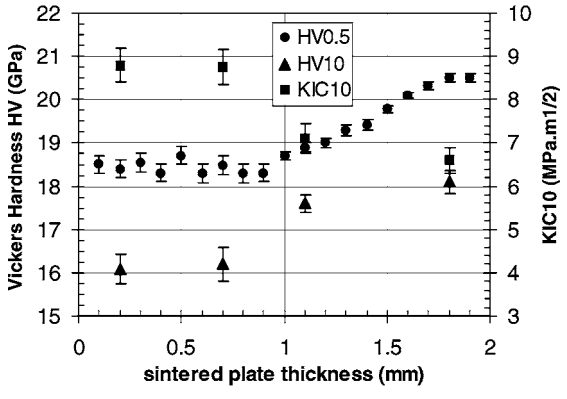

(b)

Figure 6 (a) Comparison of predicted and experimental results and (b) hardness and toughness data along the cross-sectioned WC-Co/WC-Co-Ti(C,N) FGM.

the powder suspension specific EPD characteristics. During deposition of a FGM material with a single gradient, 3 phases can be distinguished. Phase I consists of homogenous deposition of the circulating starting suspension. After a pre-defined deposition time, the second suspension is added to the circulating suspension for a given time (phase II). After addition of all powder, EPD is continued in phase III. Without going into detail into the mathematical expressions, the profile of the Ti(C,N) and/or Co gradient can be modified by changing one or more EPD parameters, such as the addition rate and addition time of the second suspension to the circulating suspension, or the concentration and volume of both powder suspensions.

Fig. 5a illustrates the change in gradient profile as a function of the addition rate 'R' of the second suspension for a WC-Co/WC-Co-Ti(C,N) FGM. In this case 50 ml of a 400 g/l WC-Co-10Ti(C,N) powder suspension was added continuously to a 50 ml circulating WC-10Co powder suspension, with a powder concentration of 300 g/l after 60 s of initial deposition of the WC-10Co suspension. EPD was continued up to a total deposition time of 300 s. By decreasing the addition rate, the slope of the gradient declined. Moreover, the maximum obtained Ti(C,N) content increased slightly from 5.9 to 6.2 wt% with decreasing addition rate. In a similar way, the influence of the powder concentration 'C' of the WC-Co-10Ti(C,N) suspension added at 0.3 ml/s was investigated as shown in Fig. 5b.

It is clear that different gradient profiles can be engineered by changing the experimental parameters. The calculated results of the EPD model [19] were verified experimentally. Therefore, a starting suspension of 300 g/l WC-10Co powder was circulated through the EPD cell for 60 s applying a voltage of 800 V. Subsequently, a second suspension of 400 g/l WC-Co-10Ti(C,N) was added continuously at 0.3 ml/s for 2 min. Afterwards, EPD was continued for 2 min. The deposit was dried, CIPed and sintered at 1450°C for 1 h. Fig. 6a shows the quantitative EPMA results along a cross-section of the plate. A very good correlation was achieved between the theoretically predicted and experimentally obtained profile. A gradient in Ti(C,N) content from 0 wt% up to 5.8 wt% is created. Vickers $HV_{0.5}$ hardness measurements along the cross-section of the sintered plate show a gradient profile in properties (Fig. 6b). HV_{10} hardness measurements were performed in the homogeneous regions on both sides. A $HV_{0.5}$ hardness gradient from 18.5 GPa up to 20.5 GPa is achieved with increasing Ti(C,N) content. HV_{10} measurements performed in the homogeneous material regions reveal values of 16.1 and 18.1 GPa respectively. Moreover, indentation toughness measurements show a reverse gradient compared to the hardness gradient. A K_{IC10} value of 6.6 $MPa \cdot m^{1/2}$ was obtained on the Ti(C,N)-rich side, whereas 8.8 $MPa \cdot m^{1/2}$ was measured on the Ti(C,N)-free side. In addition to the

experimentally created Ti(C,N) gradient, a gradient in cobalt content is obtained after sintering the WC-Co/WC-Co-Ti(C,N) FGM at 1450°C. Thereby, the liquid cobalt phase, formed at temperatures above 1320°C migrates during sintering from the high to the low Ti(C,N) side. As a result, a cobalt gradient is obtained from 7.5 wt% on the Ti(C,N)-rich side to 13 wt% on the Ti(C,N) free side. The Ti(C,N) gradient on the other hand is maintained after liquid phase sintering and can be predicted by the EPD model. Fig. 6a illustrates both Ti(C,N) and Co gradients after sintering.

3.3. Symmetrically graded WC-Co-Ti(C,N) FGMs

The EPD model [19] was used to predict the gradient profiles in symmetrically graded hardmetal plates. A plate-shaped FGM material with homogeneous Ti(C,N)-rich surface sides, intermediate gradient layers and a tough WC-10Co core was produced by EPD. In this case, a WC-Co-5Ti(C,N) powder was used as starting suspension. After deposition for 1 min, a suspension of WC-10Co powder was continuously added, decreasing the Ti(C,N) content from 5 to about 1 wt% in the core of the plate. After deposition of the homogeneous core layer, a WC-Co-10Ti(C,N) powder suspension was added in order to create a gradient from 0 up to 5 wt% on the other side of the plate.

Quantitative EPMA measurements on the sintered plates clearly reveal the double gradient in Ti(C,N) content (Fig. 7). A homogeneous Ti(C,N)-containing layer is obtained on both sides. Towards the core, a continuously decreasing Ti(C,N) concentration is achieved. A good correlation exists between the predicted profile and the experimental results. The hardness and composition profiles along cross-sectioned plates correlate well, as shown in Fig. 7. A $HV_{0.5}$ value of 20.5 GPa was obtained for the outer Ti(C,N) containing layers and 18 GPa for the homogeneous WC-Co core. No cracks or warping were observed in the FGM disc.

3.4. Al_2O_3/ZrO_2 discs with a symmetrical gradient

A symmetrical graded Al_2O_3/ZrO_2-Al_2O_3/Al_2O_3 disc was made by EPD as described in the experimental part.

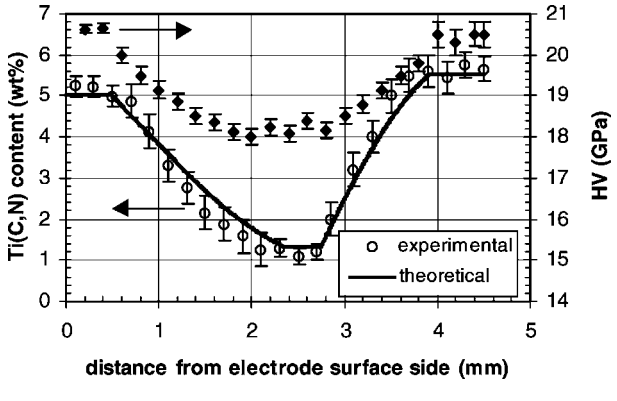

Figure 7 Ti(C,N) composition profile and Vickers hardness $HV_{0.5}$ along the cross-section of the symmetrically graded WC-Co/WC-Co-Ti(C,N) disc.

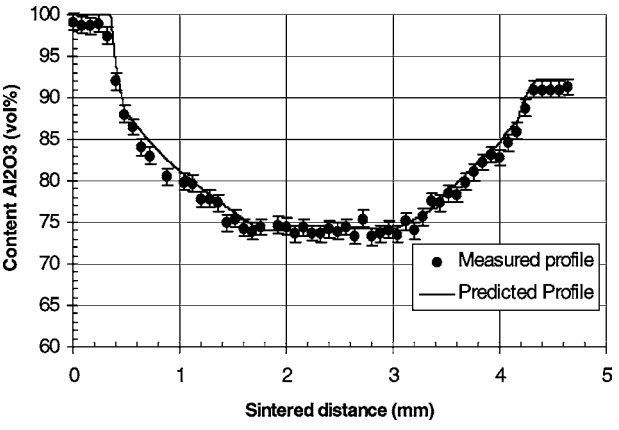

Figure 8 Measured and predicted Al_2O_3 composition profile of the FGM disc.

The measured composition profile of the FGM plate after sintering in air for 2 h at 1480°C is presented in Fig. 8, together with the predicted composition profile. Again, a good correlation is found between the experimentally measured (EPMA) and the predicted gradient from the model.

The thermally etched microstructures of the pure Al_2O_3 edge and the 80 vol% Al_2O_3 core of the graded plate are shown in Fig. 9. The ZrO_2 (white) and Al_2O_3 (grey) phases can be clearly differentiated. The ZrO_2 phase is well dispersed in the Al_2O_3 matrix in the core of the plate. No agglomerates and defects were observed in the sintered FGM disc. The Al_2O_3 grain growth limiting effect of the presence of the ZrO_2 phase is clearly illustrated by these two micrographs.

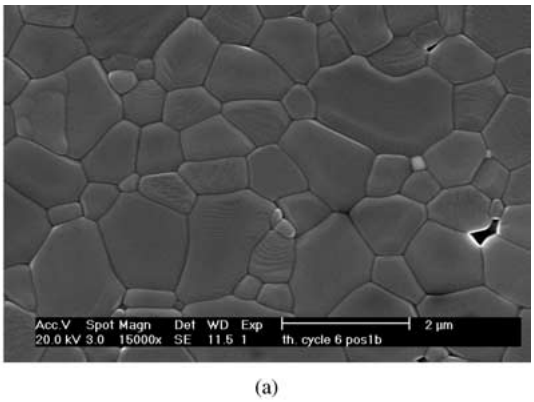

(a)

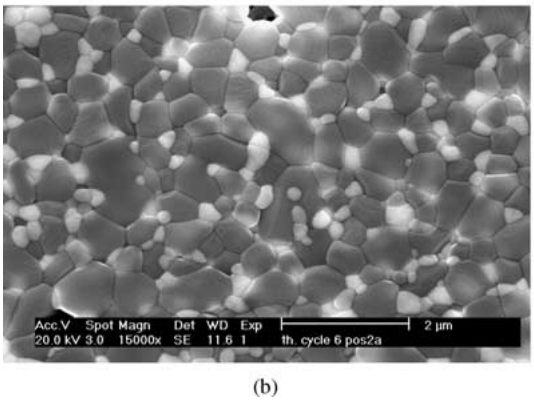

(b)

Figure 9 Scanning electron micrographs of the pure Al_2O_3 edge (a) and the 25 vol% ZrO_2 core (b) of the FGM plate. The grey phase is Al_2O_3, the white phase is ZrO_2.

Due to the lower coefficient of thermal expansion of Al_2O_3 ($\alpha = 8.4 \times 10^{-6}$) compared to ZrO_2 ($\alpha = 11 \times 10^{-6}$), compressive stresses are developed in the Al_2O_3-rich surfaces of the graded disc during cooling down from the sinter temperature. The residual stresses at the 100 vol% Al_2O_3 surface were measured with X-ray diffraction. This technique is based on the measurement of the lattice strains. It involves the measurement of minute changes in the interplanar spacing of the crystal planes from which the stress is calculated [20]. The lattice strain can be determined from the angular shift $\Delta\theta$ of X-ray diffraction profiles, where θ is the diffraction angle. The obtained strain values are then converted into stress using Hooke's law:

$$\varepsilon(\phi, \Psi) = \left(\frac{1+\nu}{E}\right)\sigma_\phi \sin^2 \Psi - \left(\frac{\sigma_\phi}{E}\right)(\sigma_{11} + \sigma_{22}) \tag{2}$$

where σ_ϕ is the stress in the ϕ-direction on the sample surface and ψ is the tilt angle of the sample surface with respect to the diffraction plane. $\sigma_\phi$can be written as:

$$\sigma_\phi = \sigma_{11}\cos^2\phi + \sigma_{22}\sin^2\phi + \sigma_{12}\sin 2\phi \tag{3}$$

with $\sigma_{11}, \sigma_{22}, \sigma_{12}$ the stresses in the plane of the plate. By measuring the peak shifts in a fixed ϕ-direction for different ψ-tilts, the linear relation between $\varepsilon(\phi,\psi)$ and $\sin^2\psi$ allows to determine σ_ϕ from the slope and $\sigma_{11} + \sigma_{22}$ from the intercept with the ordinate at $\sin^2\psi = 0$ [20]. Since the stress is measured on a cylindrical disc, it can be assumed that $\sigma_{11} = \sigma_{22}$.

The {146} reflection of α-Al_2O_3 was investigated. The ψ-tilts are respectively 24, 18.4, 0, −14.4, −26.6, −33.2, −39.2, −45, −50.8, −56.8 and −63.4. For the elastic constants ν and E, 0.27 and 356 GPa were used respectively [21]. The experimental XRD-measurements revealed a compressive stress σ_{11} of 130 $\pm$ 5 MPa in the pure Al_2O_3 surface layer of the disc with the composition profile shown in Fig. 8. By careful engineering of the widths of the constituent regions and the slope of the profiles in the graded layers in the FGM disc, it is possible to modify the compressive stress in the outer pure alumina layer of the Al_2O_3/ZrO_2 FGM discs [22].

4. Conclusions

Homogeneous ZrO_2, Al_2O_3, WC-Co and WC-Co-Ti(C,N) plates could be formed by EPD and cold isostatic pressing. These plates were fully densified by pressureless sintering. Additionally, electrophoretic deposition is shown to be a potential processing technique to create a continuous gradient in composition. Asymmetrically as well as symmetrically graded ZrO_2/Al_2O_3 and WC-Co/WC-Co-Ti(C,N) discs could be produced successfully.

An EPD model was developed for asymmetrical as well as symmetrical FGM plates. In order to predict the width and composition change of the gradient for a given material, the powder-specific EPD characteristics such as the electrophoretic mobility, the effective powder charge and the conductivity of the liquid medium have to be determined for each of the powder grades from EPD experiments on the individual homogeneous suspensions. Based on these experimental data, taking into account the EPD processing parameters and the initial concentration of the suspensions, the model allows calculating the concentration profile in the deposit as well as the sintered material, enabling to engineer the desired gradient profile in FGM materials. An excellent correlation was found between the predictions of the model and the experimental obtained profiles. It was illustrated that the model can be used in order to engineer the slope, width and microstructural composition of the gradient in ceramic as well as ceramic-metal FGM materials with single (asymmetrical) as well as double (symmetrical) gradients.

Acknowledgments

This work was supported by the Fund for Scientific Research—Flanders (No. G.0180.02), by the Flemish Institute for the Promotion of Scientific and Technological Research in Industry (IWT) under grant No. SB/993205, by the Brite-Euram program of the Commission of the European Communities under project contract No. BRPR-CT97-0505 and by the GROWTH program under project contract No. G5RD-CT2000-00354.

References

1. L. CHEN, W. LENGAUER, P. ETTMAYER, K. DREYER, H. W. DAUB and D. KASSEL, *Int. J. Refract. Met. Hard Mater.* **18** (2000) 307.
2. A. NEUBRAND and J. RODEL, *Z. Metallkd.* **88** (1997) 358.
3. A. MORTENSEN and S. SURESH, *Int. Mater. Rev.* **40** (1995) 239.
4. F. BOUYER and A. FOISSY, *J. Amer. Ceram. Soc.* **82** (1999) 2001.
5. O. VAN DER BIEST and L. VANDEPERRE, *Ann. Rev. Mater. Sci.* **29** (1999) 327.
6. C. P. GUTIERREZ, J. R. MOSLEY and T. C. WALLACE, *J. Elektrochem. Soc.* **109** (1962) 923.
7. Z. WANG, J. SCHEMILT and P. XIAO, *Scripta Mater.* **42** (2000) 653.
8. I. ZHITOMIRSKY, *J. European Ceram. Soc.* **18** (1998) 849.
9. S. PUT, J. VLEUGELS, G. ANNÉ and O.VAN DER BIEST, *Scripta Mat.* **48**(9) (2003) 1361.
10. L. VANDEPERRE and O. VAN DER BIEST, *Key Engng. Mater.* **132–136** (1997) 2013.
11. P. SARKAR, X. HUANG and P. S. NICHOLSON, *Ceram. Engin. Sci. Proc.* **14** (1993) 707.
12. S. PUT, G. ANNÉ, J. VLEUGELS and O. VAN DER BIEST, *Key Engng. Mater.* **206–213** (2002) 189.
13. C. KAWAI and S. WAKAMATSU, *J Mater. Sci. Lett.* **14** (1995) 467.
14. P. SARKAR, S. DATTA and P. S. NICHOLSON, *Composites* Part B **28B** (1997) 49.
15. S. PUT, J. VLEUGELS and O. VAN DER BIEST, *Scripta Mater.* **45** (2001) 1139.
16. P. SARKAR, X. HUANG and P. S. NICHOLSON, *J. Amer. Ceram. Soc.* **76** (1993) 1055.

17. G. R. ANSTIS, P. CHANTIKUL, B. R. LAWN and D. B. MARSHALL, *ibid.* **64** (1981) 533.
18. H. C. HAMAKER, *Trans. Faraday Soc.* **36** (1940) 279.
19. S. PUT, J. VLEUGELS and O. VAN DER BIEST, *Acta Mater.* **51**(20) (2003) 6303.
20. D. DELFOSSE, N. CHERRADI and B. ILSCHNER, *Composites* Part B **28B** (1997) 127.
21. B. D. CULLITY (Addison-Wesly, Massachusets, 1978) p. 447.
22. M. M. GASIK, B. ZHANG, O. VAN DER BIEST, J. VLEUGELS, G. ANNÉ and S. PUT, *Mater. Sci. Forum* **423–425** (2003) 23.

Received 10 December 2002
and accepted 24 February 2003